Conformational and Solvation Studies via Computer Simulation of the Novel Large Scale Diastereoselectively Synthesized Phosphinic MMP Inhibitor RXP03 Diluted in Selected Solvents

Magdalini Matziari,[†] Dimitris Dellis,[‡] Vincent Dive,[§] Athanasios Yiotakis,*[,†] and Jannis Samios*[,‡]

Department of Chemistry, Laboratory of Organic Chemistry, University of Athens, Panepistimiopolis Zografou 15771, Athens, Greece, Department of Chemistry, Laboratory of Physical Chemistry, University of Athens, Panepistimiopolis Zografou 15771, Athens, Greece, and CEA, Service D'Ingénierie Moléculaire des Protéines (SIMOPRO), Bat 152, CE-Saclay, Gif/Yvette Cedex 91191, France

Received: April 26, 2009; Revised Manuscript Received: September 12, 2009

Structure−activity relationship studies, regarding the influence of side chains of phosphinic pseudotripeptidic inhibitors on matrix metalloproteinases (MMPs), provided potent and selective inhibitors for this family of structurally and functionally related proteases. Among them, phosphinic pseudopeptide CbzPheψ[P(O)(OH)CH_2] phenylpropyl TrpNH_2, known as RXP03, has been extensively used for in vivo and in vitro studies so far. The large quantities of RXP03 required for in vivo studies, as well as the necessity for diastereoisomeric purity, motivated us to further explore and develop an efficient synthetic methodology, which allows separation of the four diastereoisomers of RXP03 based on the astonishing observed differences in solubility of the four isomers in various solvents. This fact prompted us to examine theoretically the conformational differences of these four isomers via computer simulations in the solvents used experimentally. Given the fact that the four examined diastereoisomeric forms of the phosphinic peptides exhibit different behavior in terms of potency and selectivity profiles toward zinc−metalloproteases, this theoretical study provides valuable information on the conformation of phosphinic inhibitors and therefore improves the design and synthesis of active structures. The differences in solubility of RXP03 diastereoisomers in the used solvents were examined in terms of intra- and intermolecular structure. It is found that the different solubility of the RRS and RSS diastereoisomers in EtOH is a result of the different number of hydrogen bonds formed by each isomer with EtOH molecules. In the case of SRS and SSS in Et_2O, their different solubility might be attributed to the different intramolecular hydrogen bonds formed on these diastereoisomers.

1. Introduction

Phosphinic peptides (Figure 1a) have gained significant attention during the past decade due to their inhibitory effect toward proteases, mainly zinc- and aspartyl proteases, which are implicated in numerous physiological and pathological conditions.[1] Although the phosphinyl group is a relatively weak Zn-binding group, optimized structures gain not only in potency but also mostly in selective inhibition of these enzymes.[2] Acting as transition state analogues, phosphinic peptides exhibit interesting properties for drug candidates:[3] They are devoid of toxicity, stable in vivo, and are bound to be elongated by both sides of the phosphinyl group, allowing thus optimization of the inhibitor selectivity by diversification of both primed and unprimed (P_1 and P_1') positions (Figure 1a).[4] Note also that phosphinic peptides act as potent inhibitors of many metalloproteases such as angiotensin-converting enzyme (ACE),[5] matrixins metalloproteinases (MMPs),[6,7] aminopeptidase A (APA),[8] leucine aminopeptidase,[9] etc.

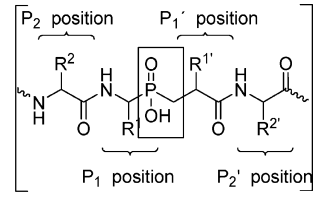

Figure 1

Figure 1. (a) Generic structure of the phosphinic inhibitors; (b) RXP03 structure. For the inhibitory potencies of RXP03 toward some MMPs, see ref 3.

Phosphinic peptides can be synthesized by using either parallel or combinatorial chemistry strategies[10,11] both in solution and on solid support.[12,13] The phosphinic pseudopeptide CbzPheψ[P(O)(OH)CH_2] phenylpropyl TrpNH_2 (RXP03) (Figure 1b) has been shown to be a potent inhibitor of MMP-2,

* Corresponding author. E-mail: isamios@chem.uoa.gr, yiotakis@chem.uoa.gr.
[†] Department of Chemistry, Laboratory of Organic Chemistry, University of Athens.
[‡] Department of Chemistry, Laboratory of Physical Chemistry, University of Athens.
[§] CEA.

10.1021/jp903830v
Published on Web 12/16/2009

MMP-8, MMP-9, MMP-11, and MMP-14 but not of MMP-1 and MMP-7. On the basis of these results, RXP03 was used in an evaluation study of the expression of the aforementioned MMPs and their TIMPs (tissue inhibitors of matrix metalloproteinases) in a rat model of liver ischemia/reperfusion.[14] In a later study, the in vivo disposition and antitumor efficacy of RXP03 was studied, revealing a dosing and scheduling influence of RXP03 on the growth of primary tumors.[15] In addition, the 3D crystal structure of the complex of the phosphinic inhibitor RXP03 in interaction with the catalytic domain of MMP-11 has been recently resolved and the results obtained provided valuable information on the conformation of this enzyme's active site.[16]

Given the fact that the four aforementioned isomers of RXP03 exhibit different inhibitory potencies against MMPs, we developed a new diastereoselective method to synthesize each of these four isomers. In addition, the fact that each isomer was found to exhibit different solubility properties motivated us to further investigate the behavior of these isomers in the solvents experimentally used, namely, ethanol (EtOH) and diethyl ether (Et_2O). To obtain insight of the different solubility of the isomer pairs, namely, RRS, RSS in EtOH, and SRS and SSS in Et_2O, obviously one needs a thorough investigation of the presumably different strength of the inter- and intramolecular interactions among solute and solvent molecules. Aiming at this goal, in the framework of the present study, we decided to employ appropriate computational techniques to explore theoretically the underlying molecular mechanisms in detail. To realize the target of this study, we used quantum mechanical calculations and molecular dynamics simulation techniques. Quantum mechanical calculations were used to optimize the geometry of each isolated isomer and further to obtain the distribution of the electrostatic charges on their atoms. On the other hand, the molecular dynamics simulation of the diluted isomer solutions led us to extract useful information concerning properties of interest.

The remainder of this paper is organized as follows. Section 2 is devoted to the experimental part of the study. In section 3, we outline the computational methods used, while, in section 4, we present and discuss the results obtained. Finally, the last section of the paper contains the main conclusions.

2. Experimental Section

2.1. Synthetic Method. As previously reported,[6] RXP03 has been synthesized using a solid-phase peptide synthesis protocol. Note however that the method proposed therein is not suitable for the requirements of a large-scale synthesis of RXP03 isomers. In order to overcome this hurdle, a new synthetic method has been developed in the framework of the present study, which according to Scheme 1 allows the separation of the four isomers of RXP03 by simple recrystallization in appropriate solvents. It should be mentioned here that the previously reported method allowed their separation only by using cumbersome chromatographic (RP-HPLC) techniques. The synthetic protocol presented herein allows the synthesis of the four diastereoisomers of RXP03 in gram scale and high yields. In detail, *R* (**1a**) and *S* (**1b**) Cbz-protected phosphinic acid analogues of phenylalanine were synthesized as a mixture of enantiomers (**1**), and they were separated using (*R*)-(+)-α-methylbenzylamine for **1a** and (*S*)-(−)-α-methylbenzylamine for **1b**.[17] Michael type addition of **1a** and **1b** to α-subsituted phenylpropyl acrylic ethylester[6] leads to the phosphinic dipeptides **2a** and **2b**, respectively. Removal of the ethylester group under basic conditions produced **3a** and **3b**. Coupling with (*S*)-$TrpNH_2$ provided the phosphinic pseudotripeptides **4a** and **4b**

SCHEME 1: Synthetic Procedure and Resolution of the Four Diastereoisomers I−IV of RXP03: (a) Resolution of 1 to 1a and 1b; (b) Michael-Type Addition to 2; (c) Saponification of 2a and 2b; (d) Coupling of 3a and 3b with $TrpNH_2$; (e) Resolution of I and II by Recrystallization in Absolute EtOH (I Insoluble, II Soluble); (f) Resolution of III and IV by Recrystallization in Et_2O (III Insoluble, IV Soluble)

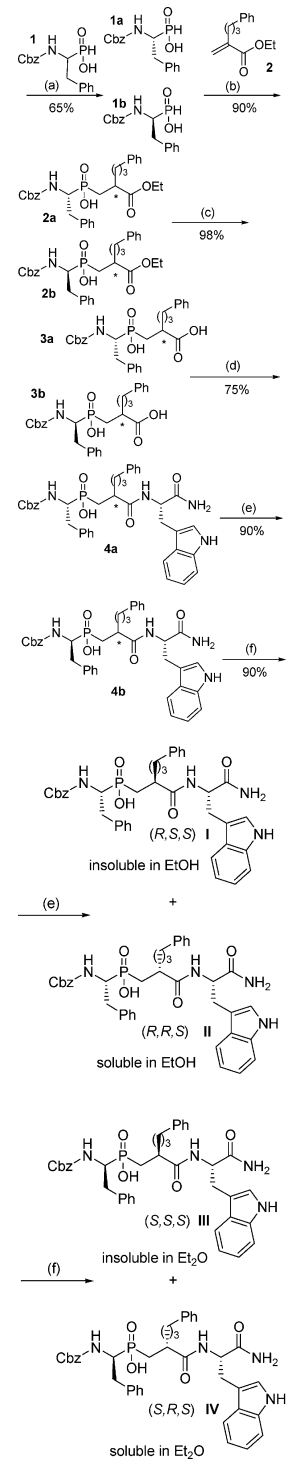

as mixtures of two pairs of isomers.[10] To our astonishment, it has been observed that each isomer proved to have different solubility properties. When, for instance, **4a** was treated with absolute ethanol (EtOH), a solid precipitated, which proved to be isomer **I**, while the filtrate consisted exclusively of isomer **II**. On the other hand, when **4b** was treated with diethyl ether

(Et_2O), isomer **III** was found to be insoluble, while **IV** was soluble in this solvent. The purity of each isomer was 99%, as obtained by using the well-known experimental techniques RP-HPLC and NMR. Finally, assignment of the absolute configuration of each isomer was performed according to methods described in detail previously.[10,18]

3. Computational Methods

3.1. General Considerations. As mentioned in the Introduction, the different solubility properties of the four RXP03 isomers obtained in various solvents in conjunction with the different inhibitory effect of each isomer toward Zn-metalloproteases[10] motivated us to investigate the conformational differences exhibiting these isomers, due to the different strength of the intra- and intermolecular interactions with solvents. The main question here is therefore under investigation: how the molecular shape of each isomer and its dynamical folding affects the characteristic parts of the isomer that are exposed to solvent molecules, leading presumably to different solubilities. We recall here that, to make clear the origin of such a behavior, the isolated molecular shape of each of the four isomers was investigated by employing a well-known geometry optimization procedure using quantum mechanical calculations. On the basis of the quantum mechanical results, we also employed the molecular dynamics (MD) simulation technique in order to make possible the interpretation of, among others, the main factors that could affect the solvation of the four isomers in the solvents used. Thus, by employing accurate potential models to describe intra- and interatomic interactions, we were able to investigate possible changes of the molecular shape of the four isomers in these solvents and, specifically, how it is affected by the presence of the solvent molecules. In addition, it was possible to reveal which parts of the isomer studied are close exposed to solvent molecules, and what kind of interactions on the atomic level are responsible for the solubility or not of the solute in the solvent under investigation. Further, possible hydrogen bonding (HB) between atoms of the diastereoisomer (intra-HB) as well as between isomer and protic solvent (inter-HB) have been systematically analyzed and interpreted.

3.2. Geometry Optimization. Geometry optimization of the isolated RXP03 isomer molecules, namely, RRS, RSS, SRS, and SSS, was performed at the DFT/B3LYP level of theory with the 6-31G* basis set. Further to this and based on the optimized molecular geometry of each of the four RXP03 isomer molecules, we calculated the distribution of the partial atomic charges of each system by using the well-known CHELPG method.[19] In summary, the CHELPG method employs a least-squares fitting procedure to determine the set of atomic partial charges of the isolated molecules that reproduces the quantum mechanical (QM) electrostatic potential at selected grid points. In this study, the constructed grid was extended to 3 Å from any of the atomic centers on the molecules and the grid spacing was set to be equal to 0.1 Å. The partial atomic charges on RXP03 molecules were calculated for all atoms of the isolated molecules except all of the $-CH_2-$ and $-CH-$ aliphatic groups and phosphinic OH that were treated as single united interaction sites. The charge on these united interaction sites was located on the center of mass of each site. The fitting procedure was subject to the constraint that the sum of the partial charges should be equal to zero for each isomer. The optimized geometry and atomic charge distribution of each isolated isomer of RXP03 obtained is summarized in Tables S1−S4 of the Supporting Information. The basis set dependence of obtained partial charges was examined by applying the same procedure using various basis sets and the HF or DFT/B3LYP levels of theory. We found that at B3LYP/6-31G* or HF/6-31G** the obtained partial charges converge. The basis set dependence of obtained partial charges of each RXP03 atom of RRS isomer is presented in Figure S2 of the Supporting Information. All QM DFT calculations were performed using the GAMESS package.[20]

3.3. Molecular Dynamics Simulations. Molecular dynamics simulation was used to study the properties of the four RXP03 stereoisomers in the solvent environment, namely, RRS and RSS in EtOH and SRS and SSS in Et_2O at room temperature and the density of each system corresponding to an atmospheric pressure of 1 atm. The Gromos96 force field[21] was used to describe intra- and intermolecular interactions between atoms of the RXP03 and solvent molecules. The Gromos forcefield includes intra- and intermolecular interactions. Intramolecular interactions include bond stretching, angle bending, proper and improper dihedral torsions, van der Waals, as well as electrostatic interactions between sites separated by three or more bonds. Intermolecular interactions include van der Waals and electrostatic interactions. The functional form of these terms is presented in eqs 1−6.

$$V_{\mathrm{vdW}}(r_{ij}) = 4\varepsilon_{ij}\left[\left(\frac{\sigma_{ij}}{r_{ij}}\right)^{12} - \left(\frac{\sigma_{ij}}{r_{ij}}\right)^{6}\right] \quad (1)$$

$$V_{\mathrm{coul}}(r_{ij}) = \frac{q_i q_j}{4\pi\varepsilon_0 r_{ij}} \quad (2)$$

$$V_{\mathrm{stretch}}(r_{ij}) = \frac{1}{4}k_{\mathrm{stretch}}({r_{ij}}^2 - {r_0}^2)^2 \quad (3)$$

$$V_{\mathrm{bend}}(\vartheta) = \frac{1}{2}k_{\mathrm{bend}}(\cos(\vartheta) - \cos(\vartheta_0))^2 \quad (4)$$

$$V_{\mathrm{impr}}(\xi) = \frac{1}{2}k_{\mathrm{impr}}(\xi - \xi_0)^2 \quad (5)$$

$$V_{\mathrm{tors}}(\varphi) = \frac{1}{2}\sum_{m=1}^{4}(k_{\mathrm{tors},m}[1 - (-1)^m \times \cos(m\varphi)]) \quad (6)$$

As mentioned above, the partial charges on interaction sites were those obtained by the QM calculations of the isomer molecules. In all cases, the cutoff distance of the nonbonded interactions was set equal to 14 Å. The long-range electrostatic interactions were described by the well-known particle mesh (PME) method.[22,23]

For each simulated molecular system, its initial configuration was prepared by placing the QM optimized structure of the RXP03 isomer molecule in the center, of a previously equilibrated solvent box. The number of the added solvent molecules was such to ensure the simulation box length to be at least 40 Å with no overlaps between solute and solvent molecules. Depending on the RXP03 isomer and solvent, this results to 710−712 EtOH and 441−494 Et_2O molecules around the solute in the simulation box. This initial solute−solvent configuration was further optimized by minimization of the simulation box potential energy using the L-BFGS minimizer,[24] followed by a 1 ns constant temperature and a pressure of 1 bar equilibration run using the Berendsen thermostat and barostat[25] with relaxation times of 0.2 and 1 ps, respectively. The resulting final configuration of the system was employed as the initial one for 10 ns NVT at 298 K extended runs using a Nose−Hoover thermostat[26,27] with a relaxation time of 0.2 ps, on which the properties of interest were calculated. The equations of motion were integrated using the leapfrog scheme[28] with a time step of 1 fs, while the intramolecular one was handled with the SHAKE method.[29] All of the systems were simulated under periodic boundary condi-

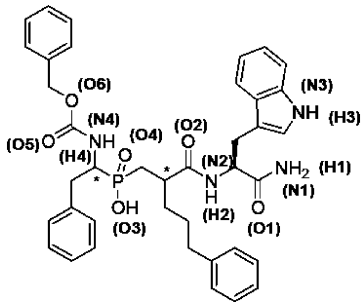

Figure 2. Two-dimensional RXP03 molecular structure with marked atoms.

tions, and the center of mass motion was removed every 0.1 ps. In addition, for each system and in order to improve the results for the potential energy surface,[30] a few 1 ns long runs were performed starting from a given configuration of RXP03 isomer prepared from a randomly perturbed initial structure. The perturbation of the initial structure was achieved by a random change of the equilibrium backbone dihedral angles up to 10°. For the two asymmetric carbon atoms of interest (see Figure 2), the possible isomerization was examined by the calculation of the dihedral angle distribution between the first side chain connected to an asymmetric carbon atom and the plane defined by the two backbone atoms connected to these carbon atoms. It was found that the distribution of these angles is centered near the equilibrium dihedral angle of each isomer, with a small width distribution. The dihedral angle distribution is presented in Figure S3 of the Supporting Information. Finally, all of the MD simulations were performed using the GROMACS package.[31]

4. Results and Discussion

4.1. Intermolecular Structure. The structure of RXP03 isomer in the EtOH and Et_2O environments was investigated using the site−site radial distribution functions $g(r)$ (RDF) between the isomers and solvent molecules. Due to the large number of site−site combinations, we will present below those that exhibit interesting features, namely, those that could support the differences in the solvation process of isomers in EtOH and Et_2O. The corresponding RDFs obtained from the simulations using the perturbed RXP03 isomer initial configurations were found to be close to those obtained from the 10 ns simulations. This is an indication that the initial configuration has a small effect on the calculated RDFs between certain sites of the four RXP03 isomers with solvents. This might be expected due to the relatively small RXP03 structure that can quickly relax close to the equilibrium structure and the fact that we deal with noncharged molecules, where the initial position of the counterions could affect the relaxation. For comparison, a few of these RDFs, namely, those that exhibit differentiation between these runs, are presented in Figure S1 of the Supporting Information.

The extent of RXP03 isomer structural changes in the solvent environment was further investigated by the calculation of the root mean squared deviation (rmsd) with respect to the initial configuration of the simulation. This initial configuration of the simulation is the configuration that results after energy minimization and equilibration in the NPT ensemble to achieve atmospheric pressure. In all cases, the backbone rmsd was found to be in the range 0.08−0.14 nm. This means that the structure of RXP03 isomers is quite stable during simulation in the solvent environment. The time dependence of the four RXP03 isomer's rmsd's in solution is presented in Figure S4 of the Supporting Information.

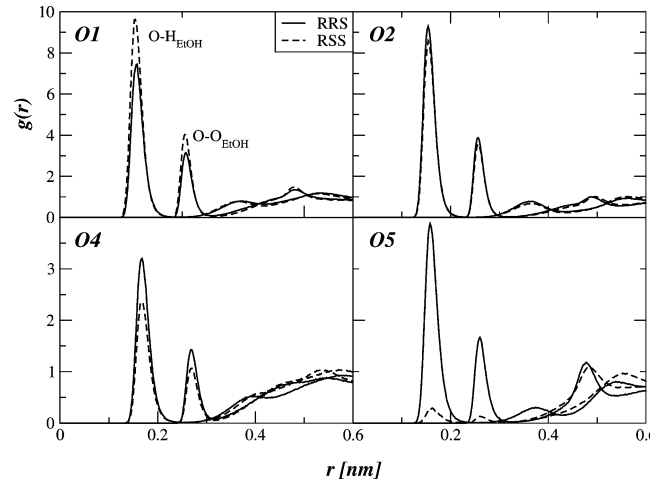

Figure 3. Calculated O−O_{EtOH} and O−H_{EtOH} RDFs. The peak at short distances is the O−H_{EtOH} RDF, and the peak at higher distances is the O−O_{EtOH} RDF.

RRS and RSS in EtOH. Since EtOH is a well-known hydrogen bonding fluid at liquid[32] and supercritical states,[33] we first investigate the RDFs between O, N and H of amino group atoms of the RRS and RSS isomers with O and H of EtOH. Due to the strong electrostatic interactions, it is expected that the EtOH molecules interact with O and NH_x sites of RXP03, obviously if they are exposed to solvent molecules. On the other hand, the aromatic groups on the solute interact mainly via van der Waals interactions with the nonpolar parts of the solvent (CH_3), if they are exposed to solvent. In Figure 2, we present the notation for O, N, and H atoms on the RXP03 molecules.

From these RDFs, those that exhibit interesting features, namely, the O1, O2, O4, and O5 oxygen atoms of RRS and RSS isomers with O and H atoms of EtOH, are presented in Figure 3. The RDFs of O3 and O6 with O and H atoms of EtOH show typical liquid-like behavior, similar for both isomers. By carefully inspecting the O−O_{EtOH} and O−H_{EtOH} RDFs (O1, O2, O4, O5) shown in Figure 3, we may observe the characteristic behavior of RDFs typical for hydrogen bonded fluids. Concretely speaking, the O−H_{EtOH} RDFs for both isomers exhibit first peaks of high amplitude located at a very short distance of 1.5−1.6 Å, while the O−O_{EtOH} RDFs reveal a lower first peak at larger correlation distances in the range 2.4−2.6 Å. However, by comparing these correlations to each other, we easily observe that the oxygen atoms O1 and O2 with O and H atoms of the EtOH molecule reveal a similar behavior for both isomers RRS and RSS. Therefore, we may conclude that RRS and RSS isomers form strong hydrogen bonds with EtOH molecules quite close to the O1 and O2 atoms.

In the case of the phosphinic oxygen atom O4, the calculated RDFs for both isomers in EtOH, exhibit first peaks of lower amplitude compared to those of O1 and O2 oxygen atoms. Note also that the correlations corresponding to the RRS isomer are higher than those of the RSS one.

It is of particular interest to discuss at this point the results obtained for the RDFs corresponding to the oxygen atom O5 (P_2 position of the molecule, see Figure 1). The corresponding RDFs show that the RRS isomer exhibits a relatively high first peak at low correlation distances in the O5−O_{EtOH} and O5−H_{EtOH} correlations, while, in the case of RSS isomer, EtOH molecules are almost absent at distances lower than 4 Å. In other words, the oxygen atom O5, as a potential candidate site to form hydrogen bonds with EtOH molecules at this position of RSS isomer, seems not to be in this particular case because

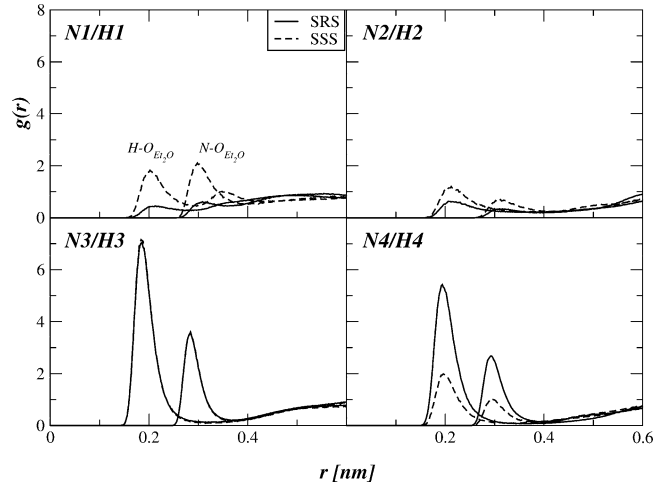

Figure 4. Calculated N−O_{Et_2O} and H−O_{Et_2OH} RDFs. The peak at short distances is the H−O_{Et_2OH} RDF, and the peak at higher distances is the N−O_{Et_2O} RDF.

our results show that this atom is probably protected from solvent molecules by aromatic rings due to the isomer three-dimensional configuration. Thus, from the above results, it is seen that the P_2 position of the RRS and RSS isomers (see Figure 1) in EtOH is affected in a different way from the solvent molecules. Concretely, the P_2 position on the RRS isomer seems to be unfolded, allowing thus the oxygen atom O5 to directly interact with EtOH solvent molecules, while in the case of the RSS isomer this position is not directly exposed to the solvent.

SRS and SSS in Et_2O. As in the case of RRS and RSS in liquid EtOH, the fact that SRS is soluble in the aprotic and not hydrogen bonding Et_2O solvent is also unclear, while this is not the case for SSS. As a first step toward elucidating this problem, we investigated the site−site RDFs between O atoms (O1−O6) and amino groups (N/H 1−4) and the center of mass of the aromatic rings of SRS and SSS isomers and the O atom and Me group on the Et_2O molecules. By carefully inspecting all of these functions, it is found that each kind of the aforementioned RDFs calculated for both isomers exhibits similar behavior except for the RDFs for the amino groups NH_x and O atom on the Et_2O molecules. Most of these RDFs show typical liquidlike behavior with small first peaks with amplitude in the range 0.8−1.5 located at moderate correlation distances, 3.6−6 Å, without unusual features. On the other hand, the calculated RDFs between the atoms of the amino groups N, H, and O on Et_2O presented in Figure 4 exhibit strong first peaks located at short correlation distances and they are different in amplitude for the two SRS and SSS isomers.

From the RDFs in Figure 4, it is easily seen that all of the H−O_{Et_2O} RDFs have their peak at a distance of 1.8−2 Å, while the N−O_{Et_2O} RDFs in the range 2.9−3 Å. This is an indication that all of the amino groups of both isomers are surrounded by Et_2O molecules oriented with their O atom toward the H atoms. From the same figure, the N3−O RDFs as well as H3−O are almost the same for both isomers, suggesting that this part in both isomers is similarly exposed to Et_2O solvent molecules. The RDFs of the rest of the N and H atoms are similar in shape, but they are different in height for each isomer. The peaks of N1/H1−O RDFs of SRS and SSS have relatively small amplitudes with those of SSS being higher. The N2/H2−O RDFs have lower peak heights than the other N/H−O_{Et_2O} RDFs for both isomers, suggesting that N2 and H2 are relatively protected from the solvent molecules probably due to the intramolecular structure. Note also that the peaks of these functions are higher in the case of SSS and lower for SRS. On the other hand, in the case of the N4/H4−O RDFs, we see a large differentiation between the two isomers SRS and SSS. These RDFs are much higher in the case of the SRS isomer compared to those of the SSS isomer. This fact suggests that, in the case of SRS isomer, more Et_2O molecules are able to be located at short distances from the N4 and H4 atoms, while, in the case of SSS isomer, it seems clearly that N4 and H4 are relatively protected from solvent molecules.

TABLE 1: Solvent Accessible Area and Its Hydrophobic and Hydrophilic Parts of RRS and RSS Isomers in EtOH and SRS and SSS in Et_2O

	EtOH		Et_2O	
	RRS	RSS	SRS	SSS
total area (nm^2)	10.42	8.74	10.43	9.53
hydrophobic area (nm^2)	7.95	6.25	8.37	7.82
hydrophilic area (nm^2)	2.47	2.49	2.06	1.71

4.2. Solvent Accessible Surface. The solvent accessible surface (SAS) of the RXP03 isomers in each solvent studied has been systematically investigated following a well-established computational procedure.[34−37] By definition, the summarized SAS of a RXP03 molecule is the outer surface that results if one draws a sphere of van der Waals radius for each atom of the solute. Thus, the corresponding SAS of each atom is a part of its sphere surface and in principle it constitutes a very small part of the whole molecular outer surface. Further, by using a well-known computational technique, we have thoroughly determined the hydrophilic as well as hydrophobic area of the aforementioned outer surface for each isomer. To this point, for a given atom on the solute molecule, we define its exposed area as hydrophilic if the absolute value of its charge is higher than 0.35|*e*|. This value for the charge ensures that aromatic rings and aliphatic sites are characterized as hydrophobic. The solvent accessible areas obtained for RRS and RSS in EtOH and SRS and SSS in Et_2O are summarized in Table 1.

From the data in Table 1, we may extract some information concerning the structure of the isomers in the solvent environment that could give insight into the different solubilities of the isomers in EtOH and Et_2O, respectively. For instance, it is found that RRS has a higher SAS than RSS in EtOH. The difference in SAS between RRS and RSS isomers in EtOH comes mainly from the increased hydrophobic part of SAS. At the atomic level, the O5 atoms of RRS and RSS isomers have an atomic SAS of 0.18 and 0.11 nm^2, respectively. This is another indication that the O5 atom of RRS isomer is more exposed than that of RSS to the EtOH molecules. On the other hand, SRS has a higher SAS than SSS isomer with higher both hydrophobic and hydrophilic SAS. At the atomic level, the N4/H4 atoms of SRS and SSS isomers, that exhibit different RDFs with the O atom of Et_2O, have an atomic SAS of 0.045/0.060 and 0.022/0.027, respectively. To conclude, the behavior of the SAS obtained in the framework of this study was found to be in agreement with the experimental solubility identified at the last stage of synthesis.

4.3. Hydrogen Bonding. ***4.3.1. Solute−Solvent Hydrogen Bonding.*** From the RDFs between the O and H atoms of EtOH and the O atoms of RRS and RSS isomers, it seems that RRS isomer forms hydrogen bonds with O1, O2, O4, and O5 atoms with EtOH. The RSS isomer seems to have the O4 atom protected from the O and H atoms in EtOH, while the rest of the O atoms seem to form hydrogen bonds with EtOH. In order to get detailed information concerning the hydrogen bonds (HBs) formed by the RRS and RSS isomers with EtOH solvent

TABLE 2: Simulated Mean Number of Hydrogen Bonds per O Atom, $\langle n_{HB} \rangle$, of RRS and RSS Isomer O Atoms with EtOH

	$\langle n_{HB} \rangle$				
system	O1	O2	O4	O5	total
RRS−EtOH	1.72	1.87	1.32	1.49	6.40
RSS−EtOH	1.00	0.97	0.87	0.14	2.98

TABLE 3: Percentage of Simulation Time Where the O and H Atoms of RXP03 Isomers Involved in Intramolecular Hydrogen Bonds Are Separated by a Distance No More Than 2.6 Å[a]

isomer	solvent	O−H pair	% of time
RRS	EtOH	O4−H1	39.5
RSS	EtOH	O4−H2	16.1
SRS	Et_2O	O2−H1	7.6
SRS	Et_2O	O4−H1	68.8
SRS	Et_2O	O4−H2	28.5
SSS	Et_2O	O2−H1	21.4
SSS	Et_2O	O4−H2	35.0
SSS	Et_2O	O2−H4	18.8

[a] Only the cases where this percentage is higher than 5% are presented.

molecules, we calculated the mean number of hydrogen bonds for the above-mentioned RXP03 O atoms. For the HB calculation, we employed the geometric definition[38,39] according to which an RXP03 O atom forms a HB with a neighboring EtOH molecule if the $O-O_{EtOH}$ and $O-H_{EtOH}$ distances are less than 3.6 and 2.5 Å, respectively, and the angle $O-O-H_{EtOH}$ is less than 30°. The mean number of HBs per O atom as well as the total number of HBs per isomer molecule obtained is presented in Table 2. From Table 2, it is clearly seen that the RRS isomer forms more HBs than the RSS one. For the O1, O2, and O4 atoms, the mean number of HBs of RRS is by a factor of 2 greater than the corresponding one of RSS. The mean number of HBs of the O5 atom is 1.49 for RRS while only 0.14 for the RSS isomer. It means that the position of the RSS isomer is protected from the EtOH molecules.

4.3.2. Intramolecular Hydrogen Bonding. The existence or not of intramolecular HBs on the isomers was investigated by the calculation of the time dependent distance between O and amino H atoms separated by three or more bonds that could form intramolecular HBs. From these functions, those that suggest the existence of intramolecular HBs are the H1−O4, H1−O2, and H2−O4 of SRS in Et_2O. We have to note here that for all four isomers in EtOH and Et_2O, transient configurations with intramolecular HBs are present, but the frequency of appearance and the duration in time of such events is found to be quite small. For instance, in the case of SRS in Et_2O environment, we found two intramolecular HBs, namely, between H1 and O2 and between H2 and O4. From the calculated time dependent distance, we have estimated the percentage of time where the involved intramolecular HBs between the O and H atoms are separated no more than 2.6 Å. The selection of this distance comes from the geometric criterion used in the calculation of HBs of RRS and RSS isomers in EtOH.[32,33,38,39] The percentage of time when the H and O atoms are involved in HBs is presented in Table 3 for the cases where it exceeds 5%. The interesting feature of these HBs is the part of the isomers where the hydrogen bonded atoms is formed. When these HBs are formed, they force a part of the backbone to form a kind of ring. This affects the orientation of the large hydrophobic side chains. This finding supports the experimental solubility of SRS isomer in Et_2O. When HBs are present, the isomer is oriented with its hydrophobic side chains toward the solvent, leading thus to increased solubility in the aprotic solvent Et_2O. Some characteristic configurations of RRS and RSS in EtOH as well as SRS and SSS in Et_2O are presented in Figure 5.

5. Conclusions

In the present study, the large quantities of RXP03 required for in vivo studies, as well as the necessity for diastereoisomeric purity, motivated us to develop an efficient synthetic method, which allows separation of the four diastereoisomers of RXP03 based on the observed differences in solubility of the four isomers in various solvents. Thus, in the framework of this

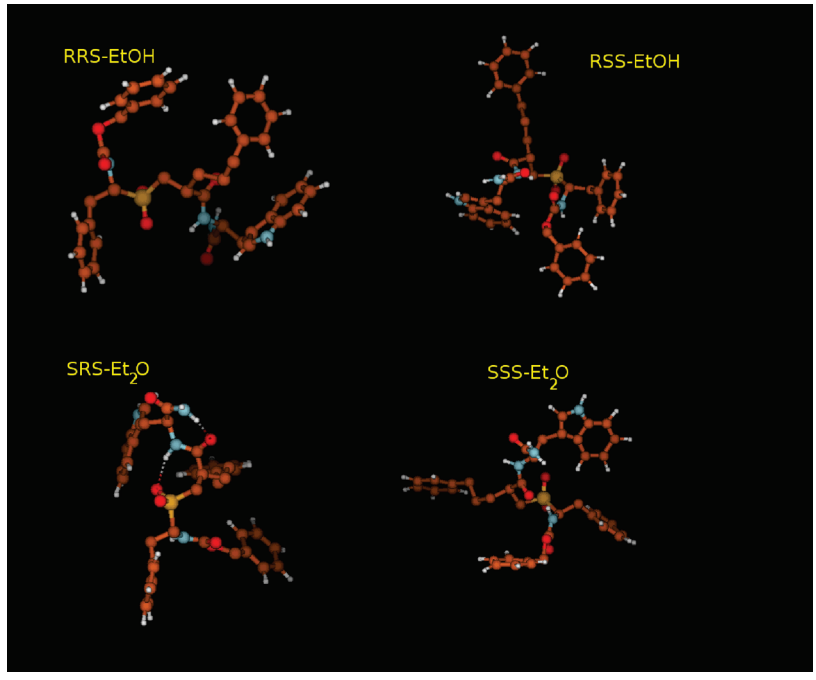

Figure 5. Characteristic structures of RRS/RSS isomers in EtOH and SRS/SSS in Et_2O.

effort, a new synthetic methodology has been undressed, which provided the four diastereoisomers of RXP03 in a large scale, high yield, and high purity. Resolution of the Cbz-protected aminophosphinic acid analogues of phenylalanine, Michael-type addition to phenylpropyl acrylic acid ethyl ester, saponification, and coupling with $TrpNH_2$ provided the four isomers, by means of recrystallization, based on the remarkable difference in solubility of the four isomers of RXP03. This fact leads us to examine theoretically the conformational differences of these four isomers via computer simulations in the solvents used experimentally.

The differences in solubility of the four RXP03 diastereoisomers in the used solvents were examined in terms of intra- and intermolecular structure in order to provide information regarding the influence of a possible conformation of the solutes on their characteristic solvation process.

Using QM calculations, the geometry of each isolated isomer molecule was first optimized and then the corresponding charge distribution was obtained. Further, the different solubility of the examined diastereoisomers in EtOH and Et_2O was investigated by means of the molecular dynamics simulation of each molecular system. The intermolecular structure between the RXP03 diastereoisomers and the solvent molecules obtained supports the experimentally found different solubilities among the isomers. All of the calculated $O-O_{EtOH}$ and $O-H_{EtOH}$ RDFs of O atoms of the RRS isomer exhibit high first peaks at very short distances with the characteristic shape showing hydrogen bonded behavior. The corresponding RDFs for the RSS isomer are similar to each other except for the P_2 position of O atom, which shows that the EtOH molecules are almost absent at short distances at this part of the isomer. The RRS isomer was found to form about six HBs with the surrounding EtOH molecules, distributed in all molecular positions that make this isomer soluble. On the other hand, the RSS isomer forms only about three HBs with EtOH but the P_2 positions of the polar atoms that potentially could form HBs with the solvent species are not accessible to them due to the fact that they are protected by the hydrophobic aromatic rings. In addition, the RRS isomer exhibits higher solvent accessible surface in EtOH compared with that for the RSS isomer. On the other hand, the SRS isomer in Et_2O has been found to form intramolecular HBs, while this does not seem to be the case for the SSS isomer. More clearly, the SRS isomer has its polar atoms protected from the nonpolar solvent, leaving their hydrophilic aromatic and aliphatic exposed to the nonpolar solvent. On the other hand, the SSS isomer does not provide such a kind of configuration because in this molecule its polar parts are protected from the solvent. As in the case of RRS/RSS in EtOH, the soluble in Et_2O SRS isomer has a higher solvent accessible area. These findings might explain the fact that the SRS isomer is soluble in Et_2O while the SSS is not.

In general, we may conclude that the different solubility of the RRS and RSS diastereoisomers in EtOH is a result of the different number of HBs formed by each isomer with EtOH molecules. In the case of SRS and SSS in Et_2O, their different solubility might be attributed to the different intramolecular HBs formed on these diastereoisomers.

Finally, in this study, the diastereoselective synthesis of the potent phosphinic inhibitor RXP03 was achieved and conformational as well as solvation studies of the RXP03 diastereoisomers were successfully performed.

Acknowledgment. This work was supported by the European Commission (FP5RDT, QLK3-CT02-02136 and FP6RDT, LSHC-CT-2003-503297), by funds from the Laboratory of Organic Chemistry, Special Account for Research Grants of National Athens University (NKUA) and by the CEA (SIMOPRO).

Supporting Information Available: Figures showing calculated radial distribution functions, ESP partial charges, dihedral angle distributions, and time evolutions, tables showing optimized geometries and fractional charges, an explanation of the general considerations, a list of abbreviations, and detailed experimental procedures. This material is available free of charge via the Internet at http://pubs.acs.org.

References and Notes

(1) Dive, V.; Georgiadis, D.; Matziari, M.; Makaritis, A.; Beau, F.; Cuniasse, P.; Yiotakis, A. *Cell. Mol. Life Sci.* **2004**, *61*, 2010–2019.

(2) Cuniasse, P.; Devel, L.; Makaritis, A.; Beau, F.; Georgiadis, D.; Matziari, M.; Yiotakis, A.; Dive, V. *Biochimie* **2005**, *87*, 393–402.

(3) Andarawewa, D. V., K. L.; Boulay, A.; Matziari, M.; Beau, F.; Guerin, E.; Rousseau, B.; Yiotakis, A.; Rio, M. C. *Int. J. Cancer* **2001**, *113*, 775–781.

(4) Schechter, I.; Berger, A. *Biochem. Biophys. Res. Commun.* **1967**, *27*, 157–162.

(5) Georgiadis, D.; Beau, F.; Czarny, B.; Cotton, J.; Yiotakis, A.; Dive, V. *Circ. Res.* **2003**, *93*, 148–154.

(6) Vassiliou, S.; Mucha, A.; Cuniasse, P.; Georgiadis, D.; Lucet-Levannier, K.; Beau, F.; Kannan, R.; Murphy, G.; Knauper, V.; Rio, M. C.; Basset, P.; Yiotakis, A.; Dive, V. *J. Med. Chem.* **1999**, *42*, 2610–2620.

(7) Schiodt, C. B.; Buchardt, J.; Terp, G. E.; Christensen, U.; Brink, M.; Berger Larsen, Y.; Meldal, M.; Foged, N. T. *Curr. Med. Chem.* **2001**, *8*, 967–976.

(8) Georgiadis, D.; Vazeux, G.; Llorens-Cortes, C.; Yiotakis, A.; Dive, V. *Biochemistry* **2000**, *39*, 1152–1155.

(9) Grembecka, J.; Mucha, A.; Cierpicki, T.; Kafarski, P. *J. Med. Chem.* **2003**, *46*, 2641–2655.

(10) Makaritis, A.; Georgiadis, D.; Dive, V.; Yiotakis, A. *Chem.—Eur. J.* **2003**, *9*, 2079–2094.

(11) Buchardt, J.; Schiodt, C. B.; Krog-Jensen, C.; Delaisse, J. M.; Foged, N. T.; Meldal, M. *J. Comb. Chem.* **2000**, *96*, 624–638.

(12) Dive, V.; Cotton, J.; Yiotakis, A.; Michaud, A.; Vassiliou, S.; Jiracek, J.; Vazeaux, G.; Chauvet, M. T.; Cuniasse, P.; Corvol, P. *Proc. Natl. Acad. Sci. U.S.A.* **1999**, *96*, 4330–4335.

(13) Jiracek, J.; Yiotakis, A.; Vincent, B.; Checler, F.; Dive, V. *J. Biol. Chem.* **1996**, *271*, 19606–19611.

(14) Cursio, R.; Mari, B.; Louis, K.; Saint-Paul, M. C.; Rostagno, P.; Giudicelli, J.; Bottero, V.; Anglard, P.; Yiotakis, A.; Dive, V.; Gugenheim, J.; Auberger, P. *FASEB J.* **2002**, *16*, 93–95.

(15) Andarawewa, D. V., K. L.; Boulay, A.; Matziari, M.; Beau, F.; Guerin, E.; Rousseau, B.; Yiotakis, A.; Rio, M. C. *Int. J. Cancer* **2001**, *113*, 775–781.

(16) Gall, A.; Ruff, M.; Kannan, R.; Cuniasse, P.; Yiotakis, A.; Dive, V.; Rio, M.; Basset, P.; Moras, D. *J. Mol. Biol.* **2001**, *307*, 577–586.

(17) Baylis, E. K.; Campbell, C. D.; Dingwall, J. D. *J. Chem. Soc., Perkin Trans.* **1984**, *1*, 2845–2853.

(18) Seco, J. M.; Quinoa, Riguera, E. *Chem. Rev.* **2004**, *104*, 17–117.

(19) Breneman, C. N.; Wiberg, K. B. *J. Comput. Chem.* **1990**, *11*, 361.

(20) Schmidt, M. W.; Baldridge, K. K.; Boatz, J. A.; Elbert, S. T.; Gordon, M. S.; Jensen, J. H.; Koseki, S.; Matsunaga, N.; Su, K. S. J.; Windus, T. L.; Dupuis, M.; Montgomery, J. A. *J. Comput. Chem.* **1993**, *14*, 1347.

(21) van Gunsteren, W. F.; Billeter, S. R.; Eising, A. A.; Hunenberger, P.; Kruger, M. A. E.; Scott, W. R. P.; Tironi, I. G. *Biomolecular Simulation: The GROMOS96 manual and user guide*; Hochschulverlag AG an der ETH Zurich: Zurich, Switzerland,1996.

(22) Darden, T.; York, D.; Pedersen, L. *J. Chem. Phys.* **1993**, *98*, 10089.

(23) Essmann, U.; Perera, L.; Berkowitz, M. L.; Darden, T.; Lee, H.; Pedersen, L. G. *J. Chem. Phys.* **1995**, *103*, 8577.

(24) Byrd, R. H.; Lu, P.; Nocedal, J. *SIAM J. Sci. Stat. Comput.* **1995**, *16*, 1190.

(25) Berendsen, H. J. C.; Postma, J. P. M.; DiNola, A.; Haak, J. R. J. *Chem. Phys.* **1984**, *81*, 3684.

(26) Nosè, S. *Mol. Phys.* **1984**, *52*, 255.

(27) Hoover, W. G. *Phys. Rev. A* **1985**, *31*, 1695.

(28) Hockney, R. W.; Goel, S. P.; Eastwood, J. *J. Comput. Phys.* **1974**, *14*, 148.

(29) Ryckaert, J. P.; Ciccotti, G.; Berendsen, H. J. C. *J. Comput. Phys.* **1977**, *23*, 327.

(30) Masella, M.; Borgis, D.; Cuniasse, P. *J. Comput. Chem.* **2008**, *29*, 1707.
(31) van der Spoel, D.; Lindahl, E.; Hess, B.; van Buuren, A. R.; Apol, E.; Meulenhoff, P. J.; Tieleman, D. P.; Sijbers, A. L. T. M.; Feenstra, K. A.; van Drunen, R.; Berendsen, H. J. C. *Gromacs User Manual version 3.3*, 2005; http://www.gromacs.org/.
(32) Saiz, L.; Padró, J. A.; Guardia, E. *Mol. Phys.* **1999**, *97*, 897.
(33) Dellis, D.; Chalaris, M.; Samios, J. *J. Phys. Chem. B* **2005**, *109*, 18575.
(34) Shrake, A.; Rupley, J. A. *J. Mol. Biol.* **1973**, *79*, 351.
(35) Eisenhaber, F.; Lijnzaad, P.; Argos, P.; Sander, C.; Scharf, M. *J. Comput. Chem.* **1995**, *16*, 273.
(36) Connolly, M. L. *J. Appl. Crystallogr.* **1983**, *16*, 548.
(37) Richmond, T. J. *J. Mol. Biol.* **1984**, *178*, 63.
(38) Jörgensen, W. L. *J. Phys. Chem.* **1986**, *90*, 1276.
(39) Ferrario, M.; Haughney, M.; McDonald, I. R.; Klein, M. L. *J. Phys. Chem.* **1990**, *93*, 5156.

JP903830V